APPLIED PHYSICS LETTERS 108, 043902 (2016)

Origins of enhanced thermoelectric power factor in topologically insulating $Bi_{0.64}Sb_{1.36}Te_3$ thin films

Wei Liu,[1,2] Hang Chi,[1] J. C. Walrath,[1] A. S. Chang,[1] Vladimir A. Stoica,[1] Lynn Endicott,[1] Xinfeng Tang,[2] R. S. Goldman,[1,3] and Ctirad Uher[1,a)]

[1]Department of Physics, University of Michigan, Ann Arbor, Michigan 48109, USA
[2]State Key Laboratory of Advanced Technology for Materials Synthesis and Processing, Wuhan University of Technology, Wuhan 430070, China
[3]Department of Materials Science and Engineering, University of Michigan, Ann Arbor, Michigan 48109, USA

(Received 4 November 2015; accepted 12 January 2016; published online 27 January 2016)

In this research, we report the enhanced thermoelectric power factor in topologically insulating thin films of $Bi_{0.64}Sb_{1.36}Te_3$ with a thickness of 6–200 nm. Measurements of scanning tunneling spectroscopy and electronic transport show that the Fermi level lies close to the valence band edge, and that the topological surface state (TSS) is electron dominated. We find that the Seebeck coefficient of the 6 nm and 15 nm thick films is dominated by the valence band, while the TSS chiefly contributes to the electrical conductivity. In contrast, the electronic transport of the reference 200 nm thick film behaves similar to bulk thermoelectric materials with low carrier concentration, implying the effect of the TSS on the electronic transport is merely prominent in the thin region. The conductivity of the 6 nm and 15 nm thick film is obviously higher than that in the 200 nm thick film owing to the highly mobile TSS conduction channel. As a consequence of the enhanced electrical conductivity and the suppressed bipolar effect in transport properties for the 6 nm thick film, an impressive power factor of about 2.0 mW m^{-1} K^{-2} is achieved at room temperature for this film. Further investigations of the electronic transport properties of TSS and interactions between TSS and the bulk band might result in a further improved thermoelectric power factor in topologically insulating $Bi_{0.64}Sb_{1.36}Te_3$ thin films.
© 2016 AIP Publishing LLC. [http://dx.doi.org/10.1063/1.4940923]

Alloys of Bi_2Te_3 with Sb_2Te_3 are the most widely studied thermoelectric (TE) materials and are the backbone of the TE technology in applications such as TE coolers and low temperature stages of power generating modules.[1–3] The performance of TE materials depends on their dimensionless figure-of-merit ZT defined as $ZT = (S^2\sigma)T/\kappa$, where S is the Seebeck coefficient, σ is the electrical conductivity, κ is the thermal conductivity, and T is the absolute temperature.[4] In order to achieve a high ZT, the material must have a high S and σ simultaneously with as low κ as possible. However, the above three transport parameters are strongly interdependent which makes it challenging to achieve very high ZT values.[5] Various attempts to improve the ZT of Bi_2Te_3-based materials have been made in the past.[6–9] A significantly reduced lattice thermal conductivity close to the amorphous limit has been demonstrated in nanostructured bulk Bi_2Te_3-based materials where ZT values of about 1.5 were reported.[8,9] Comparable gains in the TE power factor, $PF = S^2\sigma$, have not yet been achieved primarily due to a strong coupling between S and σ. A similar situation pertains to the properties of Bi_2Te_3-based thin films, except that, in general, the PF is much inferior in comparison to the bulk forms of the structure.[10–15] Thus, new approaches are needed to decouple the correlation between S and σ in order to achieve further improvements in ZT.

In the past few years, Bi_2Te_3-based materials were identified as three-dimensional topological insulators (TIs) possessing metallic topological surface states (TSS) protected by the time-reversal symmetry.[16–20] The most prominent feature of TSS is their ultra-high carrier mobility inherited from spin-momentum locking and prohibited backscattering.[16,18,20] Based on the classical TE theory, the metallic nature of TSS should not be a favorable feature with which to achieve excellent ZT values because of the speculated near-zero Seebeck coefficient.[4,5] Very recently, Xu *et al.*[21] proposed the size dependent and much improved ZT in topological insulator nanodevices due to a contribution from the two-dimensional (2D) aspects of TSS and interactions between TSS and the bulk state. Moreover, TSS could simultaneously possess a large S and a superior mobility through carefully tuning the Fermi level (E_F) position and consequently the edge-bulk interaction. Thus, the strategy of making use of the edge-bulk interaction, or utilizing the Fermi broadening arising from both the bulk and TSS contributions in a narrow energy interval, could be an approach with which to break the strong coupling between the S and the σ in TIs and thus improve the PF.[21–23] Bi_2Te_3-based films provide an ideal platform for testing the above hypothesis due to the following two reasons. First, the TSS in TIs have been well established through angle resolved photoemission spectroscopy (ARPES)[15,16,20,24] and transport measurements.[18] Second, a mature synthesis process for the growth of ultra-thin and flat Bi_2Te_3-based films with the crystallinity close to that of a single crystal has already been demonstrated.[20,25,26] In our research, we have focused on $Bi_{0.64}Sb_{1.36}Te_3$ thin films with the bulk insulating behavior, where electronic contributions from the bulk and the TSS could therefore be distinguished. We have observed a

[a)]Author to whom correspondence should be addressed. Electronic mail: cuher@umich.edu

This article is copyrighted as indicated in the article. Reuse of AIP content is subject to the terms at: http://scitation.aip.org/termsconditions. Downloaded to IP: 130.199.3.165 On: Thu, 28 Jan 2016 14:16:24

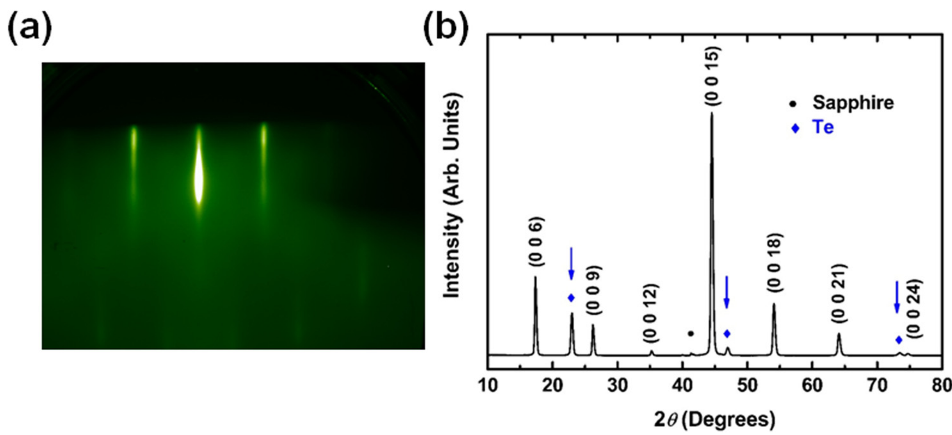

FIG. 1. Phase structure of MBE-grown $Bi_{0.64}Sb_{1.36}Te_3$ films. (a) RHEED pattern of the 6 nm thick film; and (b) XRD pattern of the 15 nm thick film with the crystalline Te capping layer.

signature of decoupling of the S from the σ through finely tuning the film thickness (6–200 nm).

$Bi_{0.64}Sb_{1.36}Te_3$ films with the thickness of 6–200 nm were grown on sapphire (0001) substrates at 500 K using molecular beam epitaxy (MBE). The growth conditions were *in-situ* monitored by Reflection High Energy Electron Diffraction (RHEED) while the film was being deposited. The film quality was *ex-situ* examined by x-ray diffraction (XRD) measurements utilizing a Rigaku Ultima IV x-ray diffractometer with Cu K_α ($\lambda = 1.5406$ Å) radiation. The composition of films was calibrated prior to the film evaporation with reference to the growth rate of binary Bi_2Te_3 and Sb_2Te_3 components under the same conditions. A 70 nm thick Te capping layer was applied onto the $Bi_{0.64}Sb_{1.36}Te_3$ thin film at room temperature subsequent to its growth in order to realize a full coverage and to protect the films from surface contamination during the exposure to air while carrying out *ex-situ* transport measurements. A pristine 6 nm $Bi_{0.64}Sb_{1.36}Te_3$ thin film was prepared under the same conditions for measuring surface topography and the E_F position via scanning tunneling microscopy (STM) and scanning tunneling spectroscopy at 100 K. The exposure of the film to the air was limited to less than 20 min during the transfer from the MBE chamber to the STM chamber. Magneto-transport measurements were carried out from 2 K to 300 K in a Quantum-Design Magnetic Property Measurement System (MPMS) using a modified probe.[15,27] The S and the σ down to 30 K were measured using a longitudinal steady-state technique in a home-made cryostat.[15,27] The uncertainty in the Hall coefficient (R_H), the σ, and the S was estimated to be $\pm 5\%$, $\pm 3\%$, and $\pm 2\%$, respectively.

Figure 1(a) presents the RHEED pattern of the 6 nm $Bi_{0.64}Sb_{1.36}Te_3$ thin film. The streaky RHEED pattern with low background intensity indicates the high quality of the film and its flat surface. The deposited $Bi_{0.64}Sb_{1.36}Te_3$ film with a 70 nm thick crystalline Te capping layer exhibited a good alignment with the substrate surface yielding intense (00l) diffractions as demonstrated in Fig. 1(b). The room temperature deposited Te layer had a preferential orientation satisfying the relation Te (100)//$Bi_{0.64}Sb_{1.36}Te_3$ (00l)//sapphire (0001). Höfer *et al.*[28] observed that the Te capping layer left the surface state band dispersion of intrinsically insulating Bi_2Te_3 films intact and the chemical potential remained unchanged as manifested via ARPES and *in situ* electrical resistivity measurements. We tested the σ of a 70 nm thick pure Te layer deposited at room temperature on the sapphire (0001) substrate and it showed a much smaller σ than the studied $Bi_{0.64}Sb_{1.36}Te_3$ films: approximately an order of magnitude lower at room temperature and over two orders of magnitude smaller below 100 K. Thus, the Te overlayer exerted a minimal influence on $Bi_{0.64}Sb_{1.36}Te_3$ films which guaranteed that the *ex situ* transport properties of $Bi_{0.64}Sb_{1.36}Te_3$ films with the Te overlayer were roughly unaffected compared to the pristine films.

Figure 2(a) displayed a large-scale STM topographic image of the 6 nm $Bi_{0.64}Sb_{1.36}Te_3$ film. The deposited film was flat over a region of several microns, without obvious pin holes, while its outermost layer was composed of islands with the height of 1 or 2 quintuple layers, confirming the layer-by-layer growth of our films. A typical plot of the differential conductance *versus* the sample bias is shown in Fig. 2(b). The effective band gap was measured to be 0.15 ± 0.10 eV,[24] with the E_F positioned near the valence band maximum (VBM). For a non-degenerate semiconductor, the electronic states within $\sim 3\ k_BT$ of the E_F were expected to dominate the σ, while the Landauer formula for S considers contributions from states within $\sim 5\ k_BT$ of the E_F. Thus, since E_F is close to the VBM, contributions to the electronic transport (σ and S) from both the bulk state and TSS could be probed simultaneously in the $Bi_{0.64}Sb_{1.36}Te_3$ film, as verified below.[22,23]

Figure 3(a) shows the magneto-resistance (MR) curves taken at 2 K for the 6 nm thick $Bi_{0.64}Sb_{1.36}Te_3$ film under different configurations of the magnetic field and the electric current. The MR under perpendicular field (the black curve) showed a remarkable cusp at around zero field, which disappeared when the field was (i) parallel to the film surface (the red curve) or (ii) parallel to the excitation current (the blue curve). In addition, ΔMR, defined as $\Delta MR = (R_B - R_0)/R_0$, under perpendicular fields of 5 T was by a factor of about 2.5 larger than ΔMR under parallel fields. The sharp MR cusp as well as the strong anisotropy of MR indicated the weak anti-localization (WAL) effect due to the strong spin-orbit coupling and a 2D nature of the magneto-transport.[26,29] We did not observe any difference in the MR when the magnetic field was parallel to the film plane and when also parallel to the current, which meant that contributions from the film's edges to the magneto-transport were slight. The results of MR measurements of this 6 nm thick $Bi_{0.64}Sb_{1.36}Te_3$ film under perpendicular fields and in the temperature range from 2 K to 100 K are summarized in Fig. 3(b). Similar to the MR

This article is copyrighted as indicated in the article. Reuse of AIP content is subject to the terms at: http://scitation.aip.org/termsconditions. Downloaded to IP: 130.199.3.165 On: Thu, 28 Jan 2016 14:16:24

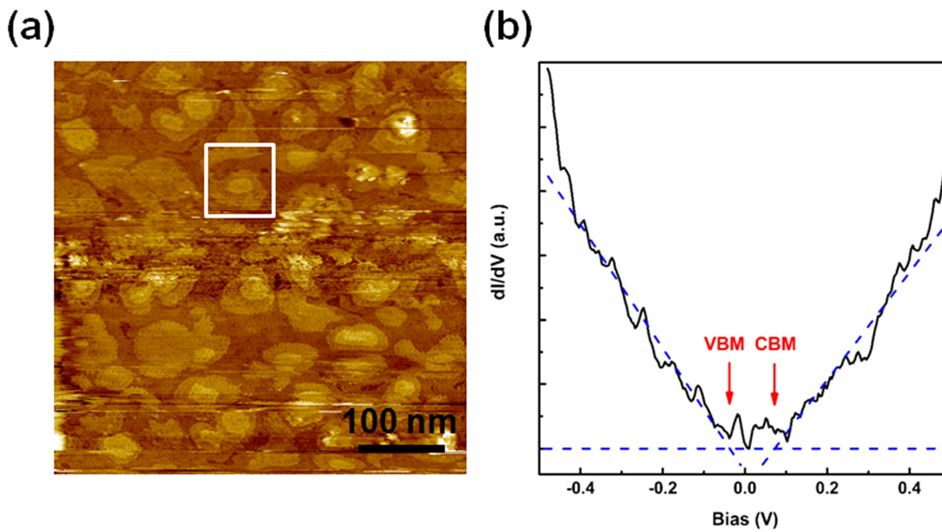

FIG. 2. (a) A large scale STM image and (b) dI/dV versus bias voltage curve of the pristine 6 nm thick $Bi_{0.64}Sb_{1.36}Te_3$ film. The white square in (a) indicates the typical island on the surface with the height of 1–2 quintuple layers. (b) The positions of the valence band minimum (VBM) and the conduction band maximum (CBM) are indicated by red arrows. The blue dashed lines are the guide to the eye for determining the change of slope of dI/dV versus bias voltage. The Fermi level (E_F) is located at the zero bias position, which is near the VBM.

at 2 K, MR at elevated temperatures showed a linear and non-saturating MR at high fields. Previous research has suggested that the non-saturated, linear-like MR resulted from the linear Dirac-like surface dispersion according to the quantum theory of linear MR.[30–32] Therefore, the WAL effect at low fields along with the linear MR at high fields has clarified the influence of the TSS on the electronic transport in $Bi_{0.64}Sb_{1.36}Te_3$ films.

The WAL effect in TIs is described by the Hikami-Larkin-Nagaoka (HLN) quantum interference model[33] and is given by

$$\Delta G = \frac{\alpha e^2}{2\pi^2\hbar}\left[\ln\left(\frac{\hbar}{4eBl_\varphi{}^2}\right) - \psi\left(\frac{1}{2} + \frac{\hbar}{4eBl_\phi{}^2}\right)\right], \quad (1)$$

where ΔG represents the magneto-conductance, e is the electronic charge, $\hbar$ is the reduced Planck's constant, l_ϕ is the phase coherence length, ψ stands for the digamma function, and α is the overall amplitude of the conductance whose expected value for a single conduction channel is 1/2.[34,35] The low field MR, within ± 1 T, studied in $Bi_{0.64}Sb_{1.36}Te_3$ films can be well fitted by this model, which is shown as the inset in Fig. 3(a). The fitting gave $\alpha \approx 1.0$ and $l_\phi \approx 110$ nm for both the 6 nm and 15 nm thick films, which matched with previous reports on the WAL effect in TIs.[25,26,34,35] Although the E_F of the bottom surface state (the surface state at the interface between the film and the substrate) is not yet known, we can reasonably conclude that TSS does contribute to the electronic transport while the number of TSS channels participating to transport properties remains unclear.

The existing 2D conduction channel, in fact, modified the electronic transport of ultra-thin $Bi_{0.64}Sb_{1.36}Te_3$ films, as shown in Figs. 4(a)–4(d). In Figs. 4(a) and 4(b), we have found that the S and the R_H possessed opposite signs up to room temperature in the 6 nm and 15 nm thick films, while this was not observed in the thick reference film[15] ($t = 200$ nm) with a similar insulating behavior, i.e., conductivity increasing with increasing temperature. In a two carrier transport system, the R_H and S are expressed by the following equations:[36,37]

$$R_H = \frac{1}{e}\frac{n_b\mu_b{}^2 \pm n_s\mu_s{}^2}{(n_b\mu_b + n_s\mu_s)^2}, \quad (2)$$

$$S = \frac{n_b\mu_b S_b + n_s\mu_s S_s}{n_b\mu_b + n_s\mu_s}, \quad (3)$$

where n and μ denote the carrier density and the carrier mobility, while the subscripts "s" and "b" indicate contributions from the TSS and the bulk state, respectively. The "-" sign is

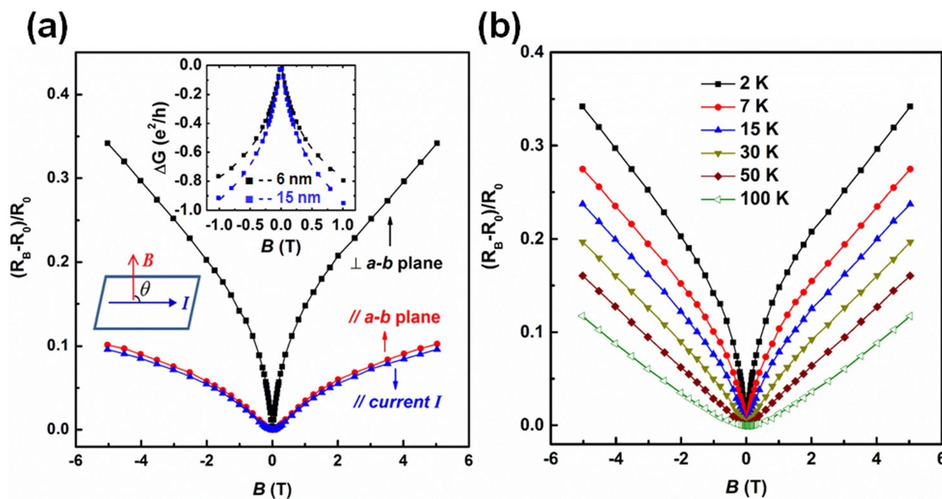

FIG. 3. MR of the 6 nm thick $Bi_{0.64}Sb_{1.36}Te_3$ film. (a) MR measured at 2 K at different field configurations: perpendicular to *a-b* plane (in black), parallel to *a-b* plane (in red) and parallel also to the current direction (in blue); (b) MR at various temperatures and under different perpendicular fields. The *a-b* plane is the abbreviation of the basal plane of $Bi_{0.64}Sb_{1.36}Te_3$ films. The inset in (a) shows the HLN fitting data (in dashed lines) and experimental results (in solid symbols), which suggests a good agreement.

This article is copyrighted as indicated in the article. Reuse of AIP content is subject to the terms at: http://scitation.aip.org/termsconditions. Downloaded to IP: 130.199.3.165 On: Thu, 28 Jan 2016 14:16:24

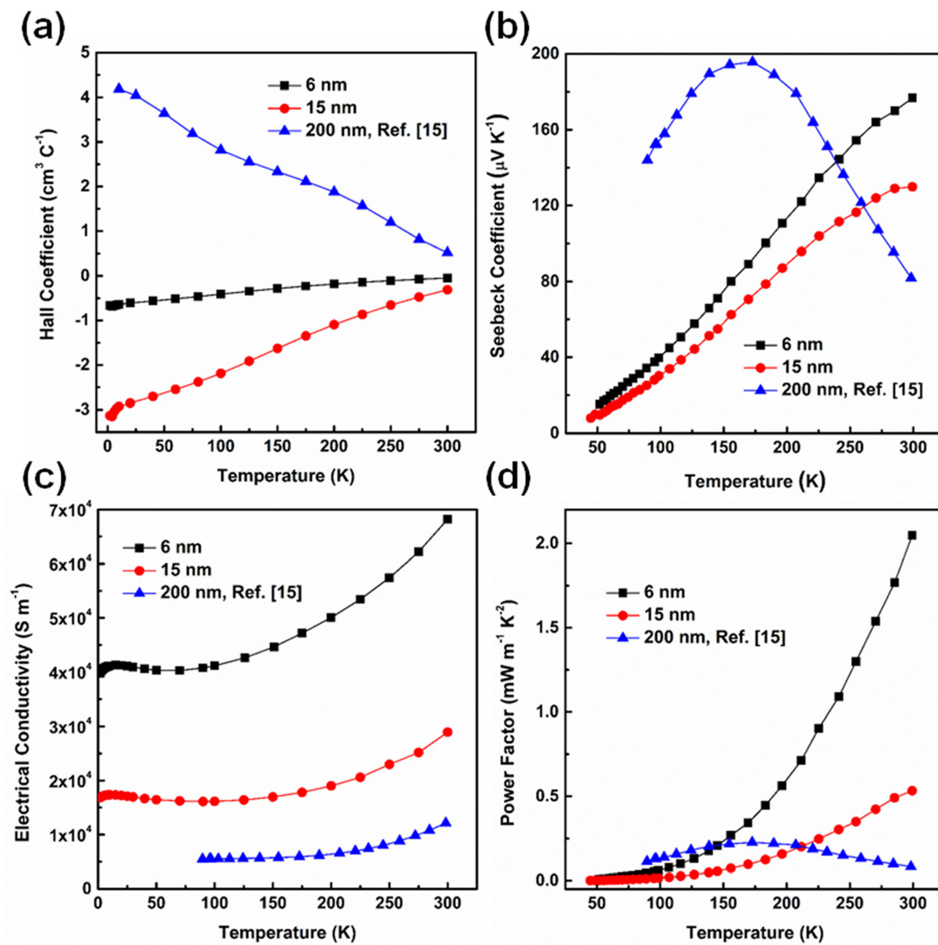

FIG. 4. Temperature dependent (a) Hall coefficient (R_H), (b) Seebeck coefficient (S), (c) electrical conductivity (σ), and (d) the power factor (PF) of $Bi_{0.64}Sb_{1.36}Te_3$ films.

selected when the TSS is filled by electrons. The E_F in $Bi_{0.64}Sb_{1.36}Te_3$ films was near the valence band edge, which determined the positive value of R_H and S_b according to the classical TE theory.[4,5] n_b was a small value due to the compensation of n- and p-type defects which resulted in a large S_b.[15,24] It is well known that the TSS possessed a remarkably large mobility due to the protection from the time reversal symmetry, verified by ARPES and by Shubnikov quantum oscillations.[16,18,20] The magnitude of the surface state mobility in BiSbTe thin films was on the order of $10^3\,cm^2\,V^{-1}\,s^{-1}$ up to room temperature, an obviously larger value than the mobility in the bulk.[4,15,18,20] Thus, the negative R_H revealed that the TSS was electron dominated and $\mu_s/\mu_b \gg n_b/n_s$. According to Fig. 4(b), the large positive S observed in 6 nm and 15 nm thick $Bi_{0.64}Sb_{1.36}Te_3$ films suggested that the S was dominated by the valence holes and the contribution from TSS was not significant. However, the sign of S_s was still not clear, since a small magnitude of S_s could well explain the sign of the S and the smaller S as compared to the reference thick film. Xu *et al.*[21] had proposed an abnormal S in TIs when E_F was located inside the band gap but close to the conduction band minimum or close to the valance band maximum due to the edge-bulk interaction. However, we observed the opposite trend of positive S and negative R_H when the E_F was close to the valence band. This implied the TSS and the bulk state dominated the magneto-transport and S, respectively.[23] The interaction between the TSS and the bulk state until now remained unclear and needed a further sophisticated analysis through carefully tuning E_F across the band gap.

As shown in Fig. 3(c), the σ of the 6 nm and 15 nm films increased by about 7 times and 2 times compared to the 200 nm thick reference film. This was related to the 2D nature of the highly conductive TSS. This was not surprising because the relative contribution from the TSS to the total conductance was enhanced with the decreasing thickness. The temperature dependence of S and σ in these films was similar to semiconducting materials with the low carrier density,[4,5] as shown in Figs. 4(b) and 4(c). Commonly, the S of Bi_2Te_3-based materials would show a turnover in the temperature dependence above 150 K due to the excitation of intrinsic carriers or the impurity level, which was the case for the thick reference film.[15] However, the S of the 6 nm and 15 nm thick $Bi_{0.64}Sb_{1.36}Te_3$ films increased monotonously with increasing temperature up to room temperature. We attributed this to the reduced film thickness and associated with it the reduced number of intrinsic defects which led to less dramatic excitations at elevated temperatures. Moreover, the 6 nm thick film possessed a larger S along with a higher σ compared to the 15 nm thick counterpart. This was likely due to a slight difference in the position of the E_F and the edge-bulk interaction. In general, the TSS strongly improved the conductivity of the ultra-thin films and the negative influence of the bipolar effect on S was suppressed, resulting in a large PF of about $2.0\,mW\,m^{-1}\,K^{-2}$ at around room temperature for the thinnest $Bi_{0.64}Sb_{1.36}Te_3$ film (see Fig. 4(d)). This was

This article is copyrighted as indicated in the article. Reuse of AIP content is subject to the terms at: http://scitation.aip.org/termsconditions. Downloaded to IP: 130.199.3.165 On: Thu, 28 Jan 2016 14:16:24

about one order of magnitude higher than the reference thick film, demonstrating the remarkable positive effect of the TSS and the reduced density of intrinsic defects on the thermoelectric power factor.

In summary, scanning tunneling microscopy and magneto-transport measurements on the bulk insulating $Bi_{0.64}Sb_{1.36}Te_3$ film manifested the existence of TSS and its effectiveness in enhancing the PF. The presence of the TSS was favorable for the electrical conductivity of films while the bipolar effect was suppressed in the ultra-thin region, resulting in the large PF of $2.0\,\mathrm{mW\,m^{-1}\,K^{-2}}$ measured for the 6 nm thick film. We also noticed that the contribution of the TSS was diminishing with the increasing film thickness. The thickness dependence of transport properties also indicated that TSS could be used to decouple the tight correlation between the S and the σ in topological insulator thin films. However, further investigations are needed to establish the effect of adjusting the E_F across the band gap of $Bi_{0.64}Sb_{1.36}Te_3$ ultra-thin films to specify the contribution of TSS towards the S and the role of the edge-bulk interaction.

The authors gratefully acknowledge the financial support from the Center for Solar and Thermal Energy Conversion, an Energy Frontier Research Center funded by the U.S. Department of Energy, Office of Science, Basic Energy Sciences under Award No. # DE-SC-0000957 and the financial support from the National Basic Research Program of China (973 program) under Project No. 2013CB632502. This material is based upon work supported by the National Science Foundation Graduate Student Research Fellowship under Grant No. DGE 1256260. R.S.G. was also supported in part by the U.S. DoE under Award No. DE-PI0000012, and A.S.C. was supported by the National Science Foundation through the Materials Research Science and Engineering Center at the University of Michigan, Grant No. DMR-1120923.

[1]J. H. Yang and C. Thierry, MRS Bull. **31**, 224 (2006).
[2]I. Chowdhury, R. Prasher, K. Lofgreen, G. Chrysler, S. Narasimhan, R. Mahajan, D. Koester, R. Alley, and R. Venkatasubramanian, Nat. Nanotechnol. **4**, 235 (2009).
[3]*Modules, Systems, and Applications in Thermoelectrics*, edited by D. M. Rowe (CRC Press, Boca Raton, FL, 2012), Vol. 2.
[4]*CRC Handbook of Thermoelectrics*, edited by D. M. Rowe (CRC Press, Boca Raton, FL, 1995).
[5]G. J. Snyder and E. S. Toberer, Nat. Mater. **7**, 105 (2008).
[6]L. D. Hicks and M. S. Dresselhaus, Phys. Rev. B **47**, 12727 (1993).
[7]R. Venkatasubramanian, E. Siivola, T. Colpitts, and B. O'Quinn, Nature **413**, 597 (2001).
[8]B. Poudel, Q. Hao, Y. Ma, Y. C. Lan, A. Minnich, B. Yu, X. Yan, D. Z. Wang, A. Muto, D. Vashaee, X. Y. Chen, J. M. Liu, M. S. Dresselhaus, G. Chen, and Z. F. Ren, Science **320**, 634 (2008).
[9]W. J. Xie, J. He, H. J. Kang, X. F. Tang, S. Zhu, M. Laver, S. Y. Wang, J. Copley, C. M. Brown, Q. J. Zhang, and T. M. Tritt, Nano Lett. **10**, 3283 (2010).
[10]L. W. D. Silva, M. Kaviany, and C. Uher, J. Appl. Phys. **97**, 114903 (2005).
[11]M. Takashiri, S. Tanaka, and K. Miyazaki, Thin Solid Films **519**, 619 (2010).
[12]A. Taylor, C. Mortensen, R. Rostek, N. Nguyen, and D. C. Johnson, J. Electron. Mater. **39**, 1981 (2010).
[13]N. Peranio, M. Winkler, D. Bessas, Z. Aabdin, J. König, H. Böttner, R. P. Hermann, and O. Eibl, J. Alloys Compd. **521**, 163 (2012).
[14]M. Stolzer, V. Bechstein, and J. Meusel, in *Proceeding of the 16th International Conference on Thermoelectrics* (ICT 1997), pp. 93–96.
[15]W. Liu, V. A. Stoica, H. Chi, L. Endicott, and C. Uher, J. Alloys Compd. **647**, 50 (2015).
[16]Y. L. Chen, J. G. Analytis, J. H. Chu, Z. K. Liu, S. K. Mo, X. L. Qi, H. J. Zhang, D. H. Lu, X. Dai, Z. Fang, S. C. Zhang, I. R. Fisher, Z. Hussain, and Z. X. Shen, Science **325**, 178 (2009).
[17]D. Hsieh, Y. Xia, D. Qian, L. Wray, F. Meier, J. H. Di, J. Osterwalder, L. Patthey, A. V. Fedorov, H. Lin, A. Bansil, D. Grauer, Y. S. Hor, R. J. Cava, and M. Z. Hasan, Phys. Rev. Lett. **103**, 146401 (2009).
[18]D. X. Qu, Y. S. Hor, J. Xiong, R. J. Cava, and N. P. Ong, Science **329**, 821 (2010).
[19]C. Z. Chang, J. S. Zhang, X. Feng, J. Shen, Z. C. Zhang, M. H. Guo, K. Li, Y. B. Ou, P. Wei, L. L. Wang, Z. Q. Ji, Y. Feng, S. H. Ji, X. Chen, J. F. Jia, X. Dai, Z. Fang, S. C. Zhang, K. He, Y. Y. Wang, L. Lu, X. C. Ma, and Q. K. Xue, Science **340**, 167 (2013).
[20]K. Hoefer, C. Becker, D. Rata, J. Swanson, P. Thalmeier, and L. H. Tjeng, Proc. Natl. Acad. Sci. U. S. A. **111**, 14979 (2014).
[21]Y. Xu, Z. X. Gan, and S. C. Zhang, Phys. Rev. Lett. **112**, 226801 (2014).
[22]D. J. Singh, Phys. Rev. B **81**, 195217 (2010).
[23]J. S. Zhang, X. Feng, Y. Xu, M. H. Guo, Z. C. Zhang, Y. B. Ou, Y. Feng, K. Li, H. J. Zhang, L. L. Wang, X. Chen, Z. X. Gan, S. C. Zhang, K. He, X. C. Ma, Q. K. Xue, and Y. Y. Wang, Phys. Rev. B **91**, 075431 (2015).
[24]J. S. Zhang, C. Z. Zhu, Z. C. Zhang, J. Wen, X. Feng, K. Li, M. H. Liu, K. He, L. L. Wang, X. Chen, Q. K. Xue, X. C. Ma, and Y. Y. Wang, Nat. Commun. **2**, 574 (2011).
[25]S. E. Harrison, S. Li, Y. Huo, B. Zhou, Y. L. Chen, and J. S. Harris, Appl. Phys. Lett. **102**, 171906 (2013).
[26]N. Bansal, Y. S. Kim, M. Brahlek, E. Edrey, and S. Oh, Phys. Rev. Lett. **109**, 116804 (2012).
[27]G. Y. Wang, L. Endicott, H. Chi, P. Lošt'ák, and C. Uher, Phys. Rev. Lett. **111**, 046803 (2013).
[28]K. Höfer, C. Becker, S. Wirth, and L. H. Tjeng, AIP Adv. **5**, 097139 (2015).
[29]B. A. Assaf, T. Cardinal, P. Wei, F. Katmis, J. S. Moodera, and D. Heiman, Appl. Phys. Lett. **102**, 012102 (2013).
[30]A. A. Abrikosov, Phys. Rev. B **58**, 2788 (1998).
[31]H. Tang, D. Liang, R. L. J. Qiu, and X. P. A. Gao, ACS Nano **5**, 7510 (2011).
[32]X. L. Wang, Y. Du, S. X. Dou, and C. Zhang, Phys. Rev. Lett. **108**, 266806 (2012).
[33]S. Hikami, A. I. Larkin, and Y. Nagaoka, Prog. Theor. Phys. **63**, 707 (1980).
[34]S. X. Zhang, R. D. McDonald, A. Shekhter, Z. X. Bi, Y. Li, Q. X. Jia, and S. T. Picraux, Appl. Phys. Lett. **101**, 202403 (2012).
[35]L. He, X. F. Kou, M. R. Lang, E. S. Choi, Y. Jiang, T. X. Nie, W. J. Jiang, Y. B. Fan, Y. Wang, F. X. Xiu, and K. L. Wang, Sci. Rep. **3**, 3406 (2013).
[36]E. H. Putley, *The Hall Effect and Related Phenomena* (Butterworth, London, 1960).
[37]Y. I. Ravich, B. A. Efimova, and I. A. Smirnov, *Semiconducting Lead Chalcogenides* (Plenum Press, New York, 1970).

This article is copyrighted as indicated in the article. Reuse of AIP content is subject to the terms at: http://scitation.aip.org/termsconditions. Downloaded to IP: 130.199.3.165 On: Thu, 28 Jan 2016 14:16:24